Research Article | Vol. 29, No. 3 / 1 February 2021 / Optics Express 3976

Optics EXPRESS

3D reconstruction of weakly scattering objects from 2D intensity-only measurements using the Wolf transform

AHMED B. AYOUB,* JOOWON LIM, ELIZABETH E. ANTOINE, AND DEMETRI PSALTIS

Ecole Polytechnique Fédérale de Lausanne, Optics Laboratory, CH-1015 Lausanne, Switzerland
ahmed.ayoub@epfl.ch

Abstract: A new approach to optical diffraction tomography (ODT) based on intensity measurements is presented. By applying the Wolf transform directly to intensity measurements, we observed unexpected behavior in the 3D reconstruction of the sample. Such a reconstruction does not explicitly represent a quantitative measure of the refractive index of the sample; however, it contains interesting qualitative information. This 3D reconstruction exhibits edge enhancement and contrast enhancement for nanostructures compared with the conventional 3D refractive index reconstruction and thus could be used to localize nanoparticles such as lipids inside a biological sample.

1. Introduction

Optical diffraction tomography (ODT) is a powerful label-free measurement tool which can be used for high-speed live imaging of transparent objects in three-dimensional space [1–10]. By acquiring 2D projections from different illumination angles and extracting their complex amplitudes, an estimate of the 3D refractive index (RI) distribution of an object can be reconstructed using inverse scattering models [10]. To obtain the complex amplitude, a digital holographic microscopy (DHM) setup is needed. An advantage of ODT over conventional phase imaging techniques is that, by recording both amplitude and phase of the scattered field, it can provide quantitative information about the sample. An alternative to using DHM to measure both the amplitude and phase at the detector is the measurement of only the intensity of the total field, which can subsequently be used to retrieve the phase. For example, phase can be inferred from non-holographic intensity measurements using the transport of intensities principle [11]. In the context of ODT, M. Maleki et al. used an iterative scheme based on the Gerchberg-Saxton algorithm (GS) [12] to retrieve the phase map from the intensity profile for each 2D projection [13]. The same group used intensity measurements to retrieve an RI estimate through a direct inversion procedure [14]. In their work, the intensity of the far-field was measured for different illumination angles. The intensity measurement includes not only a component from which the 3D object can be reconstructed, but also a twin image whose contribution to the final 3D reconstruction was negligible in their study. More recently, other works that used a direct inversion approach to retrieve the refractive index distribution out of the intensity measurements have also been demonstrated using detailed modeling of the propagation of light through the 3D sample in reflection geometry [15–17]. An alternative approach to direct inversion is a reconstruction of the 3D RI distribution of a sample from far-field intensity by using complex iterative schemes which minimize an error function [18–26]. Tian and Waller used this approach with LED illumination [21], and more recently, Pham et al. [24] used an iterative reconstruction scheme based on the Lippmann-Schwinger forward model using intensity measurements. Chowdhury et al. used a beam propagation model (BPM) as the forward model [25] to estimate the 3D refractive index from intensity-only measurements, where high-resolution reconstructions were obtained with

#414543 https://doi.org/10.1364/OE.414543
Journal © 2021 Received 9 Nov 2020; revised 21 Dec 2020; accepted 12 Jan 2021; published 25 Jan 2021

Optics EXPRESS

lateral and axial resolutions of ≤ 240 nm and ≤ 900 nm, respectively. R. Ling et al. [26] took yet another approach to intensity diffraction tomography, deriving phase and absorption transfer functions as a function of the pupil function, power of illumination beam, and the Green's function. In their work, the cost function consists of (1) the data fidelity term which is the difference between the actual measurement and the predicted measurement from the forward model and (2) Tikhonov regularization which was the l2 regularization of the permittivity. By imposing a minimum total energy constraint on the cost function, a closed form for the real and imaginary part of the permittivity by manipulating the regularization parameters. While this approach produces a refractive index measurement from intensity-only measurements, is only accounts for single scattering events and requires regularization and minimization operations.

The Wolf transform [1] is a well-known operator which maps the 2D Fourier transform of the measured field for each 2D projection onto a spherical cap in the 3D Fourier domain to reconstruct the scattering potential. Multiple 2D projections are measured, and their Fourier transform is incorporated in the 3D Fourier domain of the object. This is followed by an inverse 3D Fourier transform to reconstruct the refractive index map spatially. The *Born* reconstruction is obtained when the complex field of the 2D projections that serve as the input to the Wolf transform is used without unwrapping the phase while the *Rytov* reconstruction is obtained by utilizing the unwrapped phase [10]. In this paper, we apply the Wolf transform to the amplitude only of the total field, which can be obtained from an intensity-only measurement and obtain 3D reconstructions. We show that we obtain reconstructions whose shape is same as the *Born* and *Rytov* methods but the contrast mechanism is different, displaying a strong enhancement of nanostructures within the 3D sample. The aims of this work are to examine the effect of applying the Wolf transform on intensity-only measurements and to elucidate the physical phenomena seen in the resulting reconstructions. We provide a theoretical analysis for the twin image effect, usually seen in on-axis holography (i.e., Gabor holography) [27], which we observe using the Wolf transform. Finally, we demonstrate the effect of the twin image on the final 3D reconstruction using experimental measurements and suggest possible biological applications of the present study.

2. Principle

The experimental system we used is shown in Fig. 1. Our experimental setup is shown in Fig. 1 [28]. A diode-pumped solid-state (DPSS) 532 nm laser was used. The laser beam is spatially filtered and collimated with a pinhole and a pair of lenses. Signal and reference beams are separated in an off-axis configuration using a non-polarizing beam splitter. The signal beam illuminates the sample with oblique illuminations in a conical illumination scenario over a full 360° rotation with a resolution of 1° for a total of 361 projections, including normal incidence. Oblique illuminations are obtained using blazed gratings written on a spatial light modulator (SLM) (Holoeye; pixel size = 8 µm and resolution = 1080×1920 pixels). Higher orders from the SLM are filtered using an iris diaphragm. Using an objective lens OBJ1 (Olympus: numerical aperture = 1.4, 100X, oil immersion) as the illuminating lens, the angle of incidence on the sample is 35°. A 4f system after the sample includes an objective lens OBJ2 (Olympus: numerical aperture = 1.45, 100X, oil immersion) and a regular lens to image the sample onto the detector. For holographic detection, the signal and reference beams are combined using a non-polarizing beam splitter and projected onto a scientific complementary metal-oxide-semiconductor (sCMOS) camera (Andor Neo 5.5 sCMOS, pixel size=6.5 µm, resolution=2150×2650 pixels). HCT116 human colon cancer cells were cultured in McCoy 5A growth medium (Gibco) supplemented with 10% fetal bovine serum (Gibco). #1 coverslips were treated with a 5 µg/mL solution of fibronectin (Sigma) in phosphate-buffered saline (PBS) and air-dried at room temperature. Cells at passage 11 were detached from culture flasks using trypsin, seeded directly onto the fibronectin-treated coverslips, and incubated 24 hours in a 37C/5% CO2 atmosphere until cells

Optics EXPRESS

adhered and spread on the coverslips. Each sample was fixed for 10 minutes at room temperature in 4% paraformaldehyde in PBS, rinsed twice with PBS, and sealed with a second coverslip.

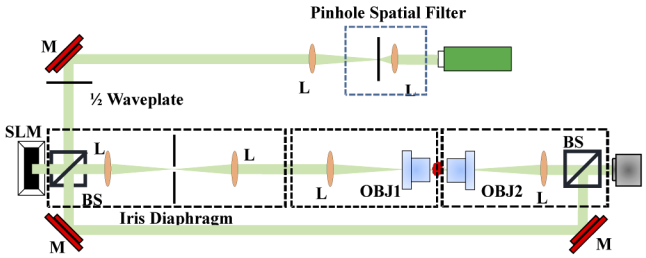

Fig. 1. Experimental tomographic setup. (M: Mirror, L: Lens, OBJ: Objective lens, BS: Beam splitter) An iris diaphragm is used to block the extra orders generated by the SLM due to its limited fill factor. 4f systems represented by the dotted rectangular blocks are used to obtain an imaging plane at the best plane of focus of the immersion objective lenses.

The 2D field incident in the detector of the ODT system is $E_t(x, y, z = z_0)$ where x, y, z are the Cartesian coordinates of the system and z_0 is the plane of best focus along the optical axis. The detected intensity is

$$|E_t|^2 = |E_i|^2 + |E_s|^2 + 2|E_i||E_s|\cos(\phi_s - \phi_i) \tag{1}$$

where $|E_t|$ is the amplitude of the total field, $|E_i|$ is the amplitude of the incident field, $|E_s|$ is the amplitude of the scattered field, and $\phi_s - \phi_i$ is the difference between the phases of the scattered and incident fields. For weakly scattering objects ($|E_s|<<|E_i|$) and defining $E_i = e^{j\phi_i}$, $|E_i| = 1$, then Eq. (1) can be rewritten as follows:

$$\begin{aligned} |E_t|^2 &\approx 1 + 2|E_s|\cos(\Delta\phi) \\ \Rightarrow |E_t| &= \sqrt{1 + 2|E_s|\cos(\Delta\phi)} \end{aligned} \tag{2}$$

where $\Delta\phi=\phi_s - \phi_i$. Due to the assumption of weakly scattering objects ($|E_s|<<1$), $|E_t|$ can be approximated as follows:

$$\begin{aligned} |E_t| &= \sqrt{1 + 2|E_s|\cos(\Delta\phi)} \\ |E_t| &\approx 1 + \frac{1}{2}(2|E_s|\cos(\Delta\phi)) \\ &= 1 + \frac{1}{2}|E_s|e^{j\Delta\phi} + \frac{1}{2}|E_s|e^{-j\Delta\phi} \end{aligned} \tag{3}$$

Multiplying both sides of Eq. (3) by $E_i = e^{j\phi_i}$, we obtain:

$$\begin{aligned} |E_t|e^{j\phi_i} &= \frac{1}{2}|E_s|e^{j\phi_s} + e^{j\phi_i} + \frac{1}{2}|E_s|e^{-j\phi_s}e^{2j\phi_i} \\ &= \frac{1}{2}E_s + e^{j\phi_i} + \frac{1}{2}E_s^*e^{2j\phi_i} \\ &= \frac{1}{2}E_s + e^{j\phi_i}(1 + \frac{1}{2}E_s^*e^{j\phi_i}) \end{aligned} \tag{4}$$

Although the term on the left-hand side of Eq. (4) is not the complex scattered field, it does include the phase information contained in the scattered field term E_s. We refer to E_s as the principal image to differentiate it from the twin image (the 3rd term in Eq. (4)). Equation (4) relates the measurement obtained from an intensity-only imaging system (i.e., $|E_t|e^{j\phi_i}$) to the information accessible only when using a holographic setup (i.e. E_s). Equation (4) includes

Optics EXPRESS

the contribution of the scattered field to the intensity measurement. However, it also contains the contributions of the twin image $\frac{1}{2}E_s{}^*e^{2j\phi_i}$ in addition to $e^{j\phi_i}$. Since $e^{j\phi_i}$ does not include the scattering effect of the sample, it does not result in any index perturbation and does not contribute to the final 3D reconstruction. We will show that under certain conditions the term $E_s{}^*e^{2j\phi_i}$ (the complex conjugate of E_s shifted by $2k_i$ in Fourier domain where $\vec{k}_i$ is the propagation vector of the incident plane wave), results in an inverted phase and negative RI contrast compared to E_s and acts approximately as a canceling term to E_s .When the numerical aperture of the optical system (OBJ2 in Fig. 1) is large enough to allow the twin image to reach the detector, then this approximate cancelation effect is most prominent for the plane of best focus. This is experimentally observed as we report later in this paper. Figure 2 demonstrates the importance of multiplying the total field amplitude $|E_t|$ (middle column) by the incident field $e^{j\phi_i}$ (right column) for correct mapping in the Fourier domain before applying the Wolf transform (c.f. Equation (4)). Although this step is not critical for reconstructions using iterative schemes as in [18,19,23–25], it is crucial for reconstructions using the Wolf transform, which relies on the direct inversion of the scattering potential. With normal incidence (top row), the scattered field $\frac{1}{2}E_s$ (solid red circle) and twin image $e^{j\phi_i}(\frac{1}{2}E_s{}^*e^{j\phi_i})$ (orange dashed circle) are both centered in the Fourier domain, overlapping. However, under oblique plane wave illumination (second and third rows), the scattered field and its twin image are both shifted off-center when the uncorrected total field is plotted (middle column). Multiplying by the incident field $e^{j\phi_i} = e^{i(\vec{k}_i\cdot\vec{r})}$ (right column) results in the scattered field remaining fixed at the center (as with normal incidence) while only the twin image is shifted. This has a profound effect on the summation of projections used to obtain the

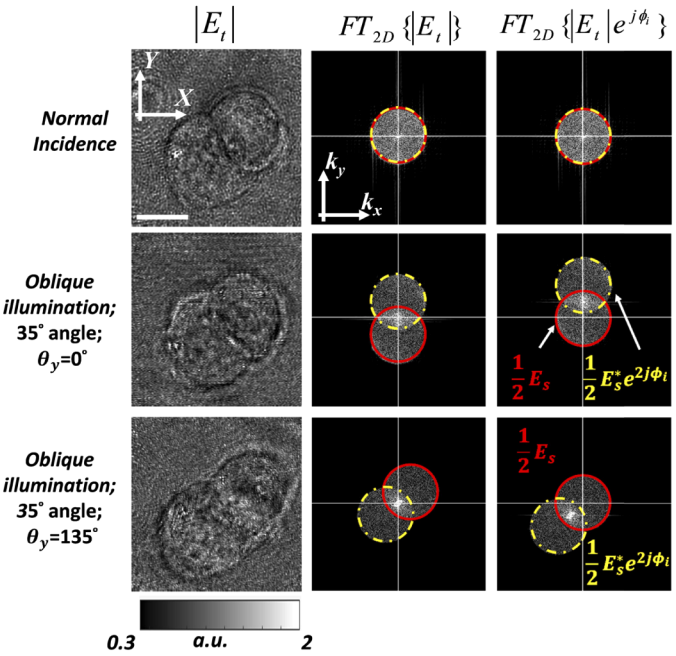

Fig. 2. The amplitude of measured total field and associated 2D Fourier transforms (logarithmic scale). The middle column shows the Fourier transform of the raw intensity map where the principal image (red circle) and the twin image (orange circle) appear concentric for normal illumination and symmetrically shifted around the origin for different oblique illuminations. The right-most column shows the Fourier transform of the raw intensity map after shifting by k_i in the frequency domain as a result of multiplying by the incident wave in the spatial domain. Scale bar = 9 µm.

Optics EXPRESS

scattering potential, as it means that the summed scattered fields are mapped correctly in 3D Fourier-space. In contrast, their twin images rotate around them according to the k-vectors of the incident field.

3. Results

The contribution of the scattered field and its twin image to the total scattering potential is demonstrated in Fig. 3 for various projections taken at different illumination angles. θ_y refers to the inclination angle of the conical illumination from the y-axis where θ_y=0 refers to $k_x = 0$ while θ_y=90 refers to k_y=0. Figure 3(A) shows the fields shown in the third column of Fig. 2 after masking out frequencies outside the limited NA of the imaging system. Figure 3(B) shows the summation over all projections when each is mapped with its own k-vector. For the scattered field ($\frac{1}{2}E_s$), all frequency components are retained by the NA filter (Fig. 3(B(I)); however, since $e^{j\phi_i}(\frac{1}{2}E_s{}^* e^{j\phi_i})$ is not centered around the origin, the high frequency components are removed by the NA of the imaging lens (OBJ2) as seen in Fig. 3(B)-II. This term therefore affects the contrast in the 3D reconstruction. See Visualization 1 and Visualization 2 for filling the frequency domain for both the principal and twin images, respectively.

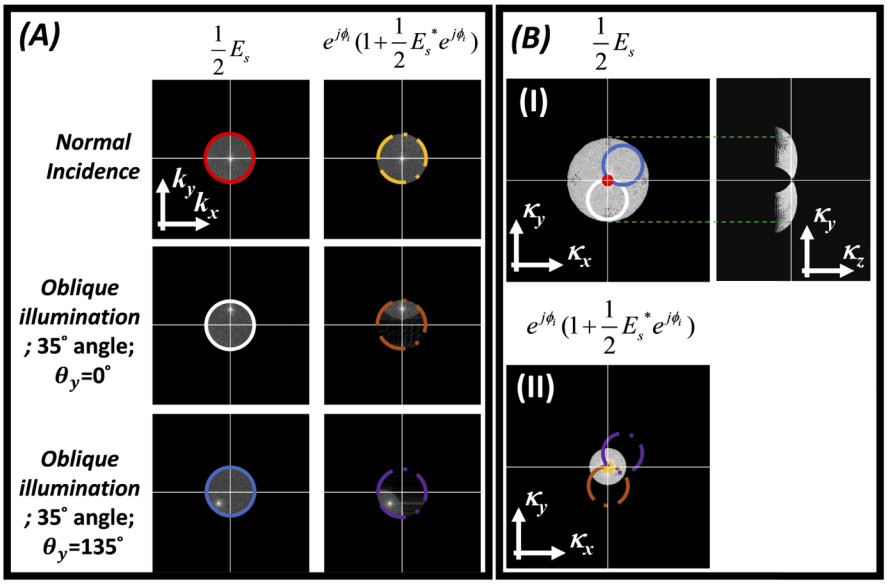

Fig. 3. (A), The spectrum of the different field components as a function of (k_x, k_y) of the scattered field (left) and its twin image (right) for different illumination angles, (B) 3D Fourier transform of the estimated scattering potential as a function of the spatial frequency components (κ_x, κ_y, κ_z) of the object plotted in 2D at κ_z = 0 for (I) the scattered fields and (II) the twin images. Panel (B) shows how the 2D projections are mapped inside the 3D Fourier space of the object where the colored circles in Panel (A) are mapped according to the incident k-vector $\vec{k}_i$. Note that the size of the scattering potential in B(I) at κ_z = 0 is not (4k*NA) as shown by the green dotted line since we are not illuminating with the maximum possible angle allowed by the numerical aperture of the objective lens.

In Fig. 4, we see the contributions of each component of the recorded field amplitude (c.f. Equation (4)) at different axial slices in the 3D reconstruction of an HCT116 cell. We first note that the reconstruction based only on $\frac{1}{2}E_s$ (Fig. 4(A), also shown in Fourier space in Fig. 3(B(I)) is materially the same as the *Born* reconstruction (scaled by ½). This reconstruction was obtained

Optics EXPRESS

using the holographic recording mode of our experimental set-up. The inverted contrast of the twin image component (Fig. 4(B)) is evident at all planes.

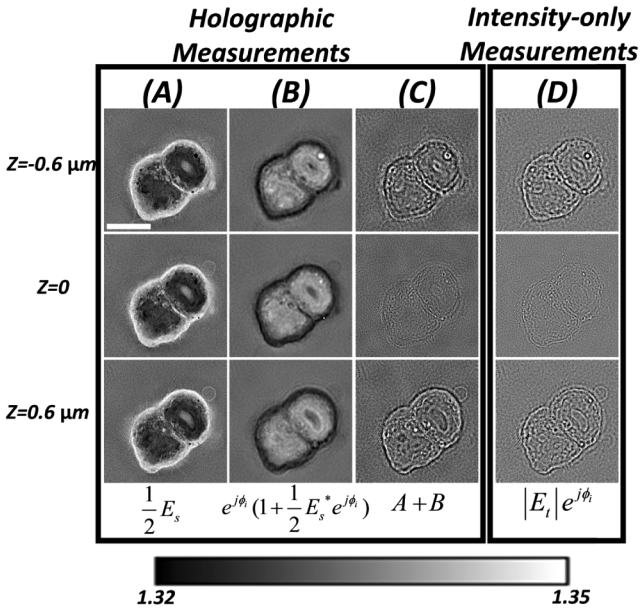

Fig. 4. HCT116 cell XY slices of 3D reconstructions at different depths obtained from (left) holographic measurements of the complex field and (right) intensity-only measurements. Columns (A), (B) and (C) were retrieved using the holographic mode in our optical setup, while column (D) represents the intensity-only measurement, Columns (C) and (D) show high structural similarity index which validate the proposed study. Scale bar = 9 µm. Colorbar shows the estimated RI map for (A) and (B) while it shows the modified refractive index map for (C) and (D) using the proposed method.

The sum of the principal image and the twin image is shown in Fig. 4(C). In the plane of best focus z=0, the low frequencies cancel one another and disappear almost entirely due to the inverted sign of the twin image. However, because the high-frequency components of the twin image are outside the NA filter (c.f. Fig. 3), this component only contributes to the low frequencies of the scattering potential, resulting in an edge-enhanced image at different planes along z (where z is the propagation direction). Figure 4(D) shows the 3D reconstruction obtained directly using intensity-only measurements as input to the Wolf transform. According to our analysis, this reconstruction is equivalent to the reconstruction obtained using the full complex field (Fig. 4(C)).We confirmed the similarity between columns C and D by calculating the structural similarity index (SSIM) [29]. The SSIM, computed for each XY slice and averaged over all slices (160 slices in our analysis), was 99 ± 0.2% over the 3D volume, quantitatively validating the approximations used to derive Eq. (4). This result demonstrates the feasibility of applying this method for intensity-only 3D reconstruction of complex samples and confirms our explanation for the qualitative observations of contrast phenomena. The observed increase in contrast as we move away from the plane of best focus is due to the fact the principal image diffracts differently from the twin image due to the conjugation. Finally, we compare our proposed intensity-only 3D reconstruction with those obtained using the classical *Born* and *Rytov* approximations (Fig. 5). As the *Born* reconstruction is retrieved by using the complex field (i.e. no phase unwrapping involved), we observed that it shows an inverted contrast in specific regions within the cell as compared to the *Rytov* reconstruction which is implemented based on the unwrapped phase. Compared to *Born* and *Rytov*, which give a quantitative estimate of the RI, the amplitude-only

Optics EXPRESS

reconstructions produce a modified RI-like measurement with artificially enhanced edges in regions of high phase gradients. For cellular imaging, this enables efficient localization of elements such as lipids and the cell membrane which are difficult to identify from RI alone. For the full z-stacks of the 3D reconstructions from *Born*, *Rytov*, and the proposed method, see Visualization 3, Visualization 4, and Visualization 5 respectively. Despite not getting the true refractive index map, the proposed technique is able to highly localize nanostructures inside the sample or on the surface (i.e. lipids in biological samples). This is demonstrated in Thomsen et al. [30], in which we used the 3D reconstructions from intensity measurements to localize Polylactic acid (PLA) particles with 200–220 nm diameter on the membranes of T-cells. These measurements were used to validate results obtained from standard fluorescence-based imaging.

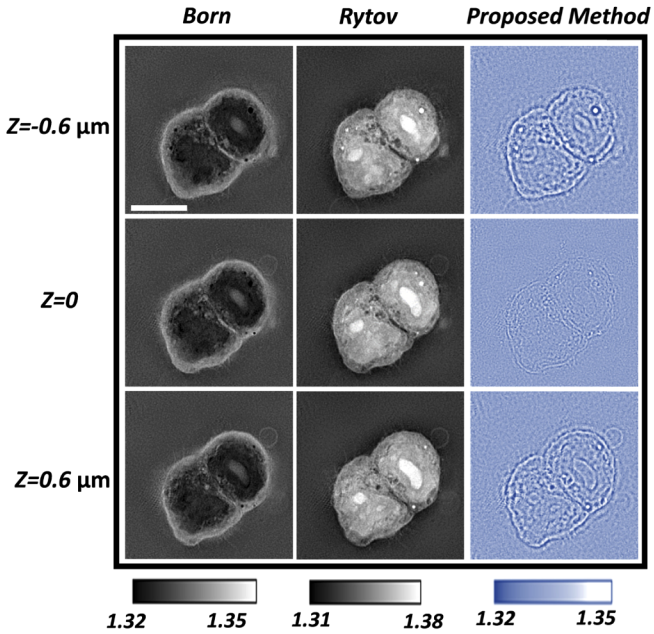

Fig. 5. HCT116 cell XY slices of 3D reconstructions at different depths obtained using *Born*, *Rytov*, and intensity-based reconstruction methods. While *Born* and *Rytov* provide a quantitative estimate of the 3D refractive index map, intensity-based reconstruction shows a modified refractive index map where only the high frequency components inside the cell (i.e. cell membrane and lipid structures). Scale bar = 9 µm.

4. Conclusion

In this paper, we proposed a new technique for the 3D reconstruction of samples using the Wolf transform from intensity measurements. Compared to other reconstruction schemes (i.e. *Born*, *Rytov*) that require optical interferometry to extract the phase, our approach is less demanding in which it only requires 2D intensity maps to perform the 3D reconstruction. As compared to [14] where the far-field intensity was detected and the twin image was neglected, in this work, the twin image was carefully analyzed and was shown to strongly affect the final reconstruction from the intensity measurements. As a result of the twin image, the 3D reconstruction from the intensity measurement resulted in the high frequency features within the sample to prevail as compared to holographic measurements. Other approaches can be followed to obtain a quantitative measure of the refractive index from intensity measurements. One approach could be to illuminate with the maximum possible angle that passes through the objective lens to minimize the effect of the

Optics EXPRESS

twin image (c.f. Supplement 1, Fig. S5), producing enhanced contrast and a quantitative measure of the RI. Another possible approach would be implementation of a neural network to map 3D RI maps (i.e. *Born, Rytov*) to the 3D reconstruction from the intensity measurement, implicitly removing the twin-image effect from the reconstructions. One limitation of neural networks is that their fidelity is strongly sample-dependent, meaning that that they must be retrained for any given class of sample (e.g. cell type, tissue type, etc.), so their utility for biological application may be limited. The proposed method is only limited to the weak scattering assumption. For multiple scattering samples, iterative reconstruction schemes can be used with forward models that take multiple scattering into account. We expect this intensity-only reconstruction to serve as an initial guess for those iterative reconstruction algorithms which usually suffer from local minima when initialized with zero values. In conclusion, we observed intriguing results by applying the Wolf transform to intensity-only measurements, obtaining edge-enhanced reconstructions when compared to complex field measurements. By using a holographic setup, we were able to investigate the physics behind this reconstruction method and compare the RI maps obtained from complex field measurements with the 3D reconstruction obtained from intensity only.

Funding. Innosuisse - Schweizerische Agentur für Innovationsförderung (34247.1 IP-ENG).

Acknowledgment. The authors would like to thank the Polymers Laboratory (LP) at EPFL and Amirhossein Saba of the Optics Lab at EPFL for fruitful discussions.

Disclosures. The authors declare no conflicts of interest.

Supplemental document. See Supplement 1 for supporting content.

References

1. E. Wolf, "Three-dimensional structure determination of semi-transparent objects from holographic data," Opt. Commun. **1**(4), 153–156 (1969).
2. Y. Sung, W. Choi, C. Fang-Yen, K. Badizadegan, R. R. Dasari, and M. S. Feld, "Optical diffraction tomography for high resolution live cell imaging," Opt. Express **17**(1), 266–277 (2009).
3. O. Haeberlé, K. Belkebir, H. Giovaninni, and A. Sentenac, "Tomographic diffractive microscopy: basics, techniques and perspectives," J. Mod. Opt. **57**(9), 686–699 (2010).
4. Y. Sung, W. Choi, N. Lue, R. R. Dasari, and Z. Yaqoob, "Stain-Free Quantification of Chromosomes in Live Cells Using Regularized Tomographic Phase Microscopy," PLOS ONE **7**(11), e49502 (2012).
5. T. Kim, R. Zhou, L. L. Goddard, and G. Popescu, "Solving inverse scattering problems in biological samples by quantitative phase imaging," Laser Photonics Rev. **10**(1), 13–39 (2016).
6. S. Shin, K. Kim, J. Yoon, and Y. Park, "Active illumination using a digital micromirror device for quantitative phase imaging," Opt. Lett. **40**(22), 5407–5410 (2015).
7. F. Charrière, A. Marian, F. Montfort, J. Kuehn, T. Colomb, E. Cuche, P. Marquet, and C. Depeursinge, "Cell refractive index tomography by digital holographic microscopy," Opt. Lett. **31**(2), 178–180 (2006).
8. K. L. Cooper, S. Oh, Y. Sung, R. R. Dasari, M. W. Kirschner, and C. J. Tabin, "Multiple phases of chondrocyte enlargement underlie differences in skeletal proportions," Nature **495**(7441), 375–378 (2013).
9. W. Choi, C. Fang-Yen, K. Badizadegan, S. Oh, N. Lue, R. R. Dasari, and M. S. Feld, "Tomographic phase microscopy," Nat. Methods **4**(9), 717–719 (2007).
10. M. Slaney, A. C. Kak, and L. E. Larsen, "Limitations of Imaging with First-Order Diffraction Tomography," IEEE Trans. Microwave Theory Tech. **32**(8), 860–874 (1984).
11. M. Beleggia, M. A. Schofield, V. V. Volkov, and Y. Zhu, "On the transport of intensity technique for phase retrieval," Ultramicroscopy **102**(1), 37–49 (2004).
12. G.-Z. Yang, B.-Z. Dong, B.-Y. Gu, J.-Y. Zhuang, and O. K. Ersoy, "Gerchberg–Saxton and Yang–Gu algorithms for phase retrieval in a nonunitary transform system: a comparison," Appl. Opt. **33**(2), 209–218 (1994).
13. M. H. Maleki and A. J. Devaney, "Phase-retrieval and intensity-only reconstruction algorithms for optical diffraction tomography," J. Opt. Soc. Am. A **10**(5), 1086–1092 (1993).
14. M. H. Maleki, A. J. Devaney, and A. Schatzberg, "Tomographic reconstruction from optical scattered intensities," J. Opt. Soc. Am. A **9**(8), 1356–1363 (1992).
15. A. Matlock, A. Sentenac, P. C. Chaumet, J. Yi, and L. Tian, "Inverse scattering for reflection intensity phase microscopy," Biomed. Opt. Express **11**(2), 911–926 (2020).
16. A. Matlock and L. Tian, "High-throughput, volumetric quantitative phase imaging with multiplexed intensity diffraction tomography," Biomed. Opt. Express **10**(12), 6432–6448 (2019).
17. J. Li, A. Matlock, Y. Li, Q. Chen, C. Zuo, and L. Tian, "High-speed in vitro intensity diffraction tomography," Adv. Photonics **1**, 33 (2019).

Optics EXPRESS

18. U. S. Kamilov, I. N. Papadopoulos, M. H. Shoreh, A. Goy, C. Vonesch, M. Unser, and D. Psaltis, "Learning approach to optical tomography," Optica **2**(6), 517–522 (2015).
19. J. Lim, A. B. Ayoub, E. E. Antoine, and D. Psaltis, "High-fidelity optical diffraction tomography of multiple scattering samples," Light: Sci. Appl. **8**(1), 82 (2019).
20. J. Lim, K. Lee, K. H. Jin, S. Shin, S. Lee, Y. Park, and J. C. Ye, "Comparative study of iterative reconstruction algorithms for missing cone problems in optical diffraction tomography," Opt. Express **23**(13), 16933–16948 (2015).
21. L. Tian and L. Waller, "3D intensity and phase imaging from light field measurements in an LED array microscope," Optica **2**(2), 104–111 (2015).
22. R. Horstmeyer, J. Chung, X. Ou, G. Zheng, and C. Yang, "Diffraction tomography with Fourier ptychography," Optica **3**(8), 827–835 (2016).
23. H. Liu, D. Liu, H. Mansour, P. T. Boufounos, L. Waller, and U. S. Kamilov, "SEAGLE: Sparsity-Driven Image Reconstruction Under Multiple Scattering," IEEE Trans. Comput. Imaging **4**(1), 73–86 (2018).
24. T.-A. Pham, E. Soubies, A. Goy, J. Lim, F. Soulez, D. Psaltis, and M. Unser, "Versatile reconstruction framework for diffraction tomography with intensity measurements and multiple scattering," Opt. Express **26**(3), 2749–2763 (2018).
25. S. Chowdhury, M. Chen, R. Eckert, D. Ren, F. Wu, N. Repina, and L. Waller, "High-resolution 3D refractive index microscopy of multiple-scattering samples from intensity images," Optica **6**(9), 1211–1219 (2019).
26. R. Ling, W. Tahir, H.-Y. Lin, H. Lee, and L. Tian, "High-throughput intensity diffraction tomography with a computational microscope," Biomed. Opt. Express **9**(5), 2130–2141 (2018).
27. D. Gabor and W. L. Bragg, "Microscopy by reconstructed wave-fronts," Proc. R. Soc. Lond. A **197**(1051), 454–487 (1949).
28. A. B. Ayoub, T.-A. Pham, J. Lim, M. Unser, and D. Psaltis, "A method for assessing the fidelity of optical diffraction tomography reconstruction methods using structured illumination," Opt. Commun. **454**, 124486 (2020).
29. W. Zhou, A. C. Bovik, H. R. Sheikh, and E. P. Simoncelli, "Image Qualify Assessment: From Error Visibility to Structural Similarity," IEEE Trans. on Image Process. **13**(4), 600–612 (2004).
30. T. Thomsen, A.B. Ayoub, D. Psaltis, and H.A. Klok, "Fluorescence-based and Fluorescent label-free Characterization of Polymer Nanoparticle Decorated T cells," Biomacromolecules (2020). Advance online publication. https://doi.org/10.1021/acs.biomac.0c00969